Outlier-Robust Manifold Pre-Integration for INS/GPS Fusion

Shin-Fang Ch'ng, Alireza Khosravian, Anh-Dzung Doan and Tat-Jun Chin

***Abstract*— We tackle the INS/GPS sensor fusion problem for pose estimation, particularly in the common setting where the INS components (IMU and magnetometer) function at much higher frequencies than GPS, and where the magnetometer and GPS are prone to giving erroneous measurements (outliers) due to magnetic disturbances and glitches. Our main contribution is a novel non-linear optimization framework that (1) fuses pre-integrated IMU and magnetometer measurements with GPS, in a manner that respects the manifold structure of the state space; and (2) supports the usage of robust norms and efficient large scale optimization to effectively mitigate the effects of outliers. Through extensive experiments, we demonstrate the superior accuracy and robustness of our approach over filtering methods (which are customarily applied in the target setting) with minimal impact to computational efficiency. Our work further illustrates the strength of optimization approaches in state estimation problems and paves the way for their adoption in the control and navigation communities.**

I. INTRODUCTION

Pose estimation is integral to robotic navigation and control systems. Recent works and surveys suggest that this problem is a subject of active research [1]–[4]. Generally, micro-electromechanical Inertial Measurement Units (IMU) are favourable for pose estimation on robotics systems due to the IMU's low weight, power consumption, and cost. IMUs (that give angular velocity and acceleration measurements) are typically combined with 3-axis magnetometers (that give partial pose information) to realise Inertial Navigation Systems (INS) that are able to give a richer set of measurements for pose estimation. However, low cost INS suffer from high noise levels and time-varying biases. Estimating robot pose based on INS dead reckoning is thus subject to drift [5].

To mitigate INS drift, a common solution is to fuse it with a GPS navigation unit that provides velocity and position measurements [6]. However, low cost GPS units are vulnerable to glitches and measurement errors, especially in areas with poor line-of-sight to the GPS satellites [7]. In fact, magnetometer measurements can also be affected by magnetic interference arising from the robot motors or the environment, leading to erroneous measurements [8]. Hence, a significant challenge in INS/GPS fusion is to exploit the relative strengths of the sensors to mitigate drift, without being biased by measurement errors or outliers.

Many sensor fusion methods have been developed and successfully deployed in navigation systems [6], [9]–[16]. Stochastic filtering techniques, especially Extended Kalman Filtering (EKF), are arguably the most common approaches for INS/GPS fusion due to their well-understood principles [17]. However, outliers will invariably lead to poor outcomes in standard EKF, which assumes that all measurements are trustworthy [7], [18], [19]. Generally speaking, designing an EKF variant that is outlier-robust and asymptotically stable for a problem with nonlinear dynamics and a state space with a Lie group structure—characteristics of our INS/GPS fusion problem—has proven to be challenging [5].

A. Handling outliers in stochastic filtering

There have been efforts to improve the robustness of classical Kalman Filtering (KF) towards outliers. The simple and common technique of discarding any observation that differs from the predicted value by a predefined threshold [19] is prone to false negatives, which can lead to the (false) build up of estimation variance and eventually poor estimates. More principled approaches developed for outlier handling in KF, such as the usage of alternative noise models [20] and Huber technique to KF residuals [21], may negatively affect the stability of the system if directly applied to INS/GPS fusion, due to the Lie group structure of the state space [2], [11].

B. Stochastic filtering on Lie groups

Recently, there has been an attention on systematically designing KFs that function intrinsically on Lie groups [3], [11]. The aim is to properly observe the underlying symmetry of the problem to enhance the convergence and stability of the filter. These efforts have led to the development of invariant KFs [11] that exhibit stronger stability properties than ad-hoc adaptations of classical KFs, especially when applied to INS/GPS fusion. However, these invariant filters do not consider measurement outliers in their design. Also, robustifying the invariant filters via the ad-hoc or heuristic approaches alluded to above seems challenging, due to the complex design and structure of these filters.

C. Nonlinear optimization in state estimation

In a parallel development, impressive results from Visual SLAM have shown that state estimation approaches based on nonlinear optimization (specifically nonlinear least squares) consistently outperform stochastic filtering methods, given the equivalent amount of computing resources [22]–[25]. In fact, nonlinear optimization can readily be brought to bear on Lie groups, and can more conveniently attain robustness against outliers by using robust norms. Yet another advantage is the availability of "generic" open source optimization packages [26]–[28] that simplify implementation.

Shin-Fang Ch'ng, Alireza Khosravian, Anh-Dzung Doan and Tat-Jun Chin are with the School of Computer Science, The University of Adelaide (shinfang.chng@adelaide.edu.au, alirezakhosravian@gmail.com, dung.doan@adelaide.edu.au, tat-jun.chin@adelaide.edu.au).

This work was supported by ARC Centre of Excellence on Robotic Vision (CE140100016).

Unsurprisingly, enthusiasm for optimization-based approaches have begun to grow in the control community, who have traditionally used stochastic filtering approaches. The recent works [29]–[32] have in fact targeted inertial navigation applications. However, these works have not considered scenarios with outliers or have systematically handled asynchronous sensor modalities (the latter is a fundamental weakness of optimization-based state estimation approaches [25]). Techniques including downsampling/interpolation [30] and averaging [31], [32] have been adopted by previous works to tackle the latter problem. However, these relatively simple strategies to handle sensor asynchrony are problematic, e.g, downsampling discards useful information, whereas the interpolation approach is dependent on the choice of the interpolation function (e.g. piecewise constant, polynomial, linear) and characteristics of the data points. If there are outliers in the data (which often occur in practice), the interpolated data creates even more problematic data. Moreover, generating interpolated data for the slower sensor will lead to a more expensive optimization problem as more variables are required to be optimized. Also, crude averaging method ignores the manifold structure of the state space.

D. Our contributions

We develop a novel non-linear optimization technique to address the state estimation problem in the INS/GPS fusion. The primary contribution of our work is the proposal of a sliding-window optimization technique which; 1) computes an accurate 6DoF robot trajectory, 2) concurrently compensate for the inherent IMU bias, 3) correctly fuse measurements from the three complementary but asynchronous sensors (IMU, magnetometer and GPS), by adapting the pre-integration approach [25] to derive the error terms associated with IMU and magnetometer that enable them to be pre-integrated across time and in a manner than respects the Lie group structure. Also, leveraging the ability of pre-integration theory to perform recursive optimization can significantly reduce the computational complexity. Our work can be seen as an extension of the pre-integration theory for visual-inertial (camera and IMU) SLAM [25] to INS/GPS fusion.

Moreover, we also explore the usage of robust norms in nonlinear least squares to effectively handle outliers from the measurements (particularly the GPS outliers), which can be easily affected by environmental factors. Our experimental results demonstrate the superior accuracy and robustness of our method over existing filtering techniques that solve the equivalent problem, i.e., INS/GPS fusion in the absence and presence of the outliers.

Note that the works closest in spirit to ours [29]–[32] have not considered outliers or have systematically handled asynchrony in the measurements, as described in Sec. I-C.

II. Problem Formulation

Consider a rigid body is equipped with an IMU, a GPS, and a magnetometer. The body-fixed frame coincides with the IMU frame, which is denoted by b. We denote the North-East-Down (NED) reference frame as w (the world frame). Neglecting the effects due to the rotation of the Earth, we assume that w is an inertial frame. The following measurements are available:

- The IMU consists of a 3-axis gyro which measures the angular velocity ${}_b\boldsymbol{\omega}$, and a 3-axis accelerometer that measures the specific acceleration ${}_b\mathbf{a}$. The sampling rate of IMU is denoted by f_{IMU}.
- The GPS unit measures the linear velocity ${}_w\mathbf{v}$ and position ${}_w\mathbf{p}$, sampled at rate f_{GPS}.
- The 3-axis magnetometer measures the magnetic field of the earth in the body-fixed frame. The magnetometer output, ${}_b\mathbf{m}$ provides partial information of the attitude matrix, $\mathbf{R}_b^w$ as:

$$ {}_b\mathbf{m} = (\mathbf{R}_b^w)^T {}_w\mathring{\mathbf{m}}, \tag{1}$$

  where ${}_w\mathring{\mathbf{m}}$ is the (approximately constant) magnetic field of the earth at the position of the rigid body expressed in the NED frame. We represent f_{Mag} as the sampling rate of magnetometer measurements.

Here we allow the sensor measurements to be asynchronous, i.e., $f_{\text{IMU}}, f_{\text{GPS}}, f_{\text{Mag}}$ can be different. By default, we assume that $f_{\text{IMU}} > f_{\text{Mag}} > f_{\text{GPS}}$, which is sensible since in most practical settings the sampling rate of IMU exceeds those of the magnetometer and GPS [30].

A. The State

Our goal is to estimate the state at time t when each GPS measurement is received up to time T. We define the state of our system as:

$$ \hat{\boldsymbol{\chi}}_t = \left(\mathbf{R}_t,\, \mathbf{v}_t,\, \mathbf{p}_t,\, \mathbf{b}_t \right), \tag{2}$$

where $(\mathbf{R}_t,\, \mathbf{p}_t) \in \text{SE(3)}$ is the pose of the rigid body, $\mathbf{v}_t \in \mathbb{R}^3$ is its linear velocity, and $\mathbf{b}_t \in \mathbb{R}^3$ is the (unknown) gyroscope bias. Here, we propose a non-linear least square formulation to minimize the sum of squared of all measurement residuals, as:

$$\begin{aligned}\min_{\hat{\boldsymbol{\chi}}_t} \frac{1}{2}\sum_{t=1}^{T} \Big(& \left\| \mathbf{r}_{\text{IMU}}(\mathbf{z}_{\text{IMU}t\to t+1}, \hat{\boldsymbol{\chi}}_t) \right\|^2_{\boldsymbol{\Sigma}_{\mathbf{i}}} + \left\| \mathbf{r}_{\text{GPS}}(\mathbf{z}_{\text{GPS}}, \hat{\boldsymbol{\chi}}_t) \right\|^2_{\boldsymbol{\Sigma}_{\mathbf{b}}} \\ & + \left\| \mathbf{r}_{\text{B}}(\mathbf{z}_{\text{B}}, \hat{\boldsymbol{\chi}}_t) \right\|^2_{\boldsymbol{\Sigma}_{\mathbf{c}}} + \left\| \mathbf{r}_{\text{Mag}}(\mathbf{z}_{\text{Mag}}, \hat{\boldsymbol{\chi}}_t) \right\|^2_{\boldsymbol{\Sigma}_{\mathbf{d}}} \Big), \end{aligned} \tag{3}$$

where $\mathbf{r}_{\text{IMU}}(\mathbf{z}_{\text{IMU}t\to t+1}, \hat{\boldsymbol{\chi}}_t)$, $\mathbf{r}_{\text{GPS}}(\mathbf{z}_{\text{GPS}}, \hat{\boldsymbol{\chi}}_t)$, $\mathbf{r}_{\text{B}}(\mathbf{z}_{\text{B}}, \hat{\boldsymbol{\chi}}_t)$ and $\mathbf{r}_{\text{Mag}}(\mathbf{z}_{\text{Mag}}, \hat{\boldsymbol{\chi}}_t)$ correspond to residuals for IMU, GPS, IMU bias and magnetometer measurements, respectively. Detailed definition of each residual term will be presented in Sec. III-A, III-B, III-C, III-E.

B. IMU model

The IMU measures angular velocity and linear acceleration of b frame relative to w frame. We assume that raw gyroscope measurements, ${}_b\tilde{\boldsymbol{\omega}}$ is affected by a slowly varying

sensor bias $\mathbf{b}^g$ [25]: [1]

$$ {}_b\tilde{\boldsymbol{\omega}}_n = {}_b\boldsymbol{\omega}_n + \mathbf{b}_n^g \tag{4} $$

$$ {}_b\tilde{\mathbf{a}}_n = \mathbf{R}_{b_n}^{w^T}({}_w\mathbf{a}_n - {}_w\mathbf{g}), \tag{5} $$

where ${}_b\boldsymbol{\omega} \in \mathbb{R}^3$ is the instantaneous angular velocity of b relative to w expressed in coordinate frame b, ${}_w\mathbf{a} \in \mathbb{R}^3$ is the instantaneous linear acceleration of b relative to w expressed in w, and ${}_w\mathbf{g}$ is the constant gravitational acceleration vector in w frame.

We employ the following continuous-time model [25]:

$$ {}_w\dot{\mathbf{p}} = {}_w\mathbf{v}, \quad {}_w\dot{\mathbf{v}} = {}_w\mathbf{a}, \quad \dot{\mathbf{R}}_b^w = \mathbf{R}_b^w {}_b\boldsymbol{\omega}_\times, \tag{6} $$

where the operator $(.)_\times$ maps a vector in $\mathbb{R}^3$ to its associated skew symmetric matrix in $\mathfrak{so}(3)$.

Assuming that ${}_b\boldsymbol{\omega}$ and ${}_w\mathbf{a}$ are constant between two time instants $n = i$ and $n = i+1$, Euler integration is applied to (6) to propagate the rigid body's pose and velocity using IMU measurements, yielding:

$$ {}_w\mathbf{p}_{i+1} = {}_w\mathbf{p}_i + {}_w\mathbf{v}_i\Delta t + \frac{1}{2}(\mathbf{R}_{b_i}^w {}_b\tilde{\mathbf{a}}_i + {}_w\mathbf{g})\Delta t^2 \tag{7a} $$

$$ {}_w\mathbf{v}_{i+1} = {}_w\mathbf{v}_i + (\mathbf{R}_{b_i}^w {}_b\tilde{\mathbf{a}}_i + {}_w\mathbf{g})\Delta t \tag{7b} $$

$$ \mathbf{R}_{b_{i+1}}^w = \mathbf{R}_{b_i}^w \exp\left(({}_b\tilde{\boldsymbol{\omega}}_i - \mathbf{b}_i^g)_\times \Delta t\right), \tag{7c} $$

where $\exp : \mathfrak{so}(3) \rightarrow$ SO(3). Although more sophisticated numerical integrated methods can be employed [35]–[38], our experiments suggest that the above Euler approximation performs very well for our specific application where IMU sampling rate is high [39].

C. Pre-integration of IMU on manifold

In this section, to simplify the presentation and without loss of generality, we assume $f_{\text{GPS}} = f_{\text{Mag}}$ and $f_{\text{GPS}}, f_{\text{Mag}} < f_{\text{IMU}}$. We further generalize this in Sec. III-E.

We initialize a state variable (i.e. a node in the optimization) of the form (2) each time we receive a GPS measurement. Our goal in this section is to combine all of the IMU measurements received between successive GPS measurements and generate a single pre-integrated IMU measurement. This pre-integration significantly reduces the computational complexity of the least squares problem (3) since it prevents re-incorporating all of the IMU measurements at each iteration of the least-squares problem.

Assume that two consecutive GPS measurements are received at times $t = i$ and $t = j$. We, hence, initialize two state variables (i.e. two nodes of the optimization) according to (2) at times $t = i$ and j. Inspired by [25], we summarize all the IMU measurements between the two required states $\hat{\boldsymbol{\chi}}_i$ and $\hat{\boldsymbol{\chi}}_j$ (to be estimated).

We denote the pre-integrate position, velocity, and orientation from $t = i$ to $t = j$ by $\Delta\mathbf{p}_{i\rightarrow j}^{b_i}, \Delta\mathbf{v}_{i\rightarrow j}^{b_i}, \Delta\mathbf{R}_{b_{i\rightarrow j}}^{b_i}$, respectively, to represent the relative motion increments between two consecutive poses and velocities. The pre-integrated delta components are initialized as $\Delta\mathbf{p}_{i\rightarrow i}^{b_i} = 0, \Delta\mathbf{v}_{i\rightarrow i}^{b_i} = 0, \Delta\mathbf{R}_{b_{i\rightarrow i}}^{b_i} = \text{I}$. By taking b_i as the reference frame, successive application of (7) between $t = i$ and $t = j$ yields

$$ \Delta\mathbf{p}_{i\rightarrow j}^{b_i} = \sum_{t=i}^{j-1}\left[\Delta\mathbf{v}_t^{b_i}\Delta t + \frac{1}{2}\Delta\mathbf{R}_t^{b_i}(\tilde{\mathbf{a}}_t)\Delta t^2\right] \tag{8a} $$

$$ \Delta\mathbf{v}_{i\rightarrow j}^{b_i} = \sum_{t=i}^{j-1}\Delta\mathbf{R}_t^{b_i}(\tilde{\mathbf{a}}_t)\Delta t \tag{8b} $$

$$ \Delta\mathbf{R}_{b_{i\rightarrow j}}^{b_i} = \prod_{t=i}^{j-1}\left(\exp\left(\tilde{\boldsymbol{\omega}}_t - \mathbf{b}_t^g\right)_\times \Delta t\right), \tag{8c} $$

where i is the discrete sample of one IMU measurement within $t = [i, j]$, and Δt is the time interval between two IMU measurements i and $i+1$.

Note that (8) is now independent of the estimated states which prevents re-calculation whenever pose and velocity estimates change, except for the bias. To avoid repeating the same equations in our paper, please find the 1st order Taylor expansion presented in [25] for the recursive implementations when the bias estimate changes. We remark that adapting the pre-integration strategy [25] in tackling asynchrony sensor modalities is conceptually superior over [30]–[32].

III. Measurement Residual Terms

In this section, we introduce our residual error terms of IMU, GPS, bias and magnetometer measurements.

A. Preintegrated IMU Factor

Given the pre-integrated measurement model in (8), we can further rewrite (7), which yields:

$$ \Delta\mathbf{p}_{i\rightarrow j}^{b_i} \doteq (\mathbf{R}_{b_i}^w)^T({}_w\mathbf{p}_j - {}_w\mathbf{p}_i - {}_w\mathbf{v}_i\Delta t_{ij} - \frac{1}{2}\mathbf{g}\,\Delta {t_{ij}}^2) \tag{9a} $$

$$ \Delta\mathbf{v}_{i\rightarrow j}^{b_i} \doteq (\mathbf{R}_{b_i}^w)^T({}_w\mathbf{v}_j - {}_w\mathbf{v}_i - \mathbf{g}\,\Delta t_{ij}) \tag{9b} $$

$$ \Delta\mathbf{R}_{b_{i\rightarrow j}}^{b_i} \doteq (\mathbf{R}_{b_i}^w)^T\mathbf{R}_{b_j}^w, \tag{9c} $$

where $\Delta t_{ij} = \sum_{t=i}^{j}\Delta t$.

We express the residual error $\mathbf{r}_{\text{IMU}}(\mathbf{z}_{\text{IMU}i\rightarrow j}, \hat{\boldsymbol{\chi}}_i) \doteq [\mathbf{e}_{\Delta\mathbf{p}_{i\rightarrow j}}, \mathbf{e}_{\Delta\mathbf{v}_{i\rightarrow j}}, \mathbf{e}_{\Delta\mathbf{R}_{i\rightarrow j}}]^T \in \mathbb{R}^9$ as:

$$ \mathbf{e}_{\Delta\mathbf{p}_{i\rightarrow j}} = (\mathbf{R}_{b_i}^w)^T({}_w\mathbf{p}_j - {}_w\mathbf{p}_i - {}_w\mathbf{v}_i\Delta t_{ij} - \frac{1}{2}\mathbf{g}\,\Delta t_{ij}^2) - \Delta\mathbf{p}_{i\rightarrow j}^{b_i} \tag{10a} $$

$$ \mathbf{e}_{\Delta\mathbf{v}_{i\rightarrow j}} = (\mathbf{R}_{b_i}^w)^T({}_w\mathbf{v}_j - {}_w\mathbf{v}_i - \mathbf{g}\,\Delta t_{ij}) - \Delta\mathbf{v}_{i\rightarrow j}^{b_i} \tag{10b} $$

$$ \mathbf{e}_{\Delta\mathbf{R}_{i\rightarrow j}} = \mathbf{q}_v\left(\mathbf{R}_{b_i}^w(\mathbf{R}_{b_j}^w)^T\Delta\mathbf{R}_{b_{i\rightarrow j}}^{b_i}\right), \tag{10c} $$

where the notation $\mathbf{q}_v(\mathbf{R}) \in \mathbb{R}^3$ denotes the vector part of the quaternion representation of $\mathbf{R} \in$ SO(3) [5], [40].

B. GPS measurement residual

GPS measurements, namely ${}_w\tilde{\mathbf{v}}_t$ and ${}_w\tilde{\mathbf{p}}_t$ received at time $t = i$ have direct relationship with the estimated states. Hence, we can construct the algebraic equation for the residual error $\mathbf{r}_{\text{GPS}}(\mathbf{z}_{\text{GPS}}, \hat{\boldsymbol{\chi}}_t) \doteq [\mathbf{e}_{\mathbf{v}_i}, \mathbf{e}_{\mathbf{p}_i}]^T \in \mathbb{R}^6$ at $t = i$ as:

$$ \mathbf{e}_{\mathbf{v}i} = {}_w\mathbf{v}_i - {}_w\tilde{\mathbf{v}}_i, \quad \mathbf{e}_{\mathbf{p}_i} = {}_w\mathbf{p}_i - {}_w\tilde{\mathbf{p}}_i. \tag{11} $$

[1] We opt not to incorporate the accelerometer bias compensation as adding an unknown accelerometer bias to (5) (on top of the unknown gyro bias) our problem setup would introduce unobservable modes, that in turn might lead to instability/divergence of the optimization solution [33], [34]. This is of particular importance in our scenario where we consider measurement outliers in addition to the bias.

C. Bias model

Since we assume the gyro measurement in the IMU is corrupted with a slow time-varying bias, this unknown bias must be estimated and compensated to achieve asymptotically accurate estimation [2], [5]. Here, we model the bias as a "random walk", resulting from the integration of the white noise.

$$\dot{\mathbf{b}}_t^g = \eta^{bg}. \tag{12}$$

By integrating (12) over successive discrete time samples $t = [i, j]$, we can form the bias residual error term, $\mathbf{r}_{\mathrm{B}}(\mathbf{z}_{\mathrm{B}}, \hat{\boldsymbol{\chi}}_t) \doteq \mathbf{e}_{\mathbf{B}i} \in \mathbb{R}^3$ as:

$$\mathbf{e}_{\mathbf{B}i} = \mathbf{b}_j^g - \mathbf{b}_i^g \,. \tag{13}$$

D. Magnetometer measurement residual

Given the magnetometer model presented in (1), we can naturally form the residual error of magnetometer measurement at time $t = i$ as:

$$\mathbf{r}_{\mathrm{Mag}}(\mathbf{z}_{\mathrm{Mag}}, \hat{\boldsymbol{\chi}}_t) \doteq \mathbf{e}_{\mathbf{M}_i} = {}_b\tilde{\mathbf{m}}_i - (\mathbf{R}_{b_i}^w)^T {}_w\mathring{\mathbf{m}}_i, \tag{14}$$

where $\mathbf{e}_{\mathbf{M}_i} \in \mathbb{R}^3$.

E. Incorporating intermediate magnetometer measurements

In Sec. II-C, we assume that the sampling rate of magnetometer is the same as the sampling rate of GPS, such that $f_{\mathrm{Mag}} = f_{\mathrm{GPS}}$. Nevertheless, in most practical scenarios, we have $f_{\mathrm{Mag}} > f_{\mathrm{GPS}}$. In this section, we generalize our proposed optimization framework to allow $f_{\mathrm{Mag}} > f_{\mathrm{GPS}}$. Inspired by the recursive predictor theory proposed by [2, Chapter 4] that compensates delays and sampling effects in pose estimation, we propose an approach that allows the incorporation of sensory data with various sampling rates into the least-squares optimization.

Assume that two consecutive GPS measurements are received at time $t = i$ and $t = j$, and a magnetometer measurement ${}_b\tilde{\mathbf{m}}_k$ is received at the time $t = k$ where $i \leq k \leq j$. The nodes $\hat{\boldsymbol{\chi}}_i$ and $\hat{\boldsymbol{\chi}}_j$ exist in the optimization, but the node $\hat{\boldsymbol{\chi}}_k$ does not exist because no GPS measurement is received at time k. Hence, it is not possible to use the magnetometer residual as proposed by (14). Instead, we, use (9c) to obtain $\mathbf{R}_{b_k}^w = \mathbf{R}_{b_i}^w \Delta\mathbf{R}_{b_{i\to k}}^{b_i}$ where $\Delta\mathbf{R}_{b_{i\to k}}^{b_i}$ is the pre-integrated orientation which can be computed using gyro measurements from $t = i$ to $t = k$ according to (8c). Replacing for ${}_b\mathbf{m}_k = \mathbf{R}_{b_k}^{w^T} {}_w\mathring{\mathbf{m}}_k$ and using (14), we obtain

$$\begin{aligned}\mathbf{e}_{\mathbf{M}_k} &= {}_b\tilde{\mathbf{m}}_k - \left(\mathbf{R}_{b_k}^w\right)^T {}_w\mathring{\mathbf{m}}_k \\ &= {}_b\tilde{\mathbf{m}}_k - \left(\Delta\mathbf{R}_{b_{i\to k}}^{b_i}\right)^T \left(\mathbf{R}_{b_i}^w\right)^T {}_w\mathring{\mathbf{m}}_k. \end{aligned} \tag{15}$$

It is now possible to implement the residual term (15) in the least-squares to incorporate the intermittent magnetometer measurements ${}_b\tilde{\mathbf{m}}_k$. Note that the residual error (15) relies on the available state $\hat{\boldsymbol{\chi}}_i$ rather than the unavailable state $\hat{\boldsymbol{\chi}}_k$. A similar methodology to the approach presented above has been proposed in [41] to mitigate asynchrony between IMU and LIDAR measurements, albeit in a different problem setup to the present paper. We remark that this concept can be employed to tackle GPS measurement delay problem. For slower GPS measurement rate, one can also consider to apply associated concept to perform the state estimation at a higher sampling rate to achieve real-time compliant applications.

IV. Handling Outliers

In practice, sensor measurements are often corrupted by outliers. From statistical point of view, an outlier is a measurement which significantly deviates from other candidates of the distribution in which it is sampled. Realistically, outliers are often derived from unmodeled factors or bizarre causes, such as temporary sensor failure, erroneous measurements or transient environment disturbance.

Generally, least square function is highly vulnerable to these outliers as a single outlier can drastically pull the estimation arbitrarily far away from the true solution [42]. This is of particular crucial importance for the INS/GPS fusion since high amplitude GPS glitches can often occur in practice, e.g. due to blockage of signals or multi-path. Also, sudden magnetic disturbance may occur in aerial vehicles, e.g. while passing from the proximity of power lines, causing temporary outliers in the magnetometer readings.

Since we are targeting a setting where we have a sequence of time-dependent variables (pose, velocity, bias) to estimate, the interaction and evolution of the variables across time are vital aspects of the problem. Therefore, our approach determine the outliers by exploring the M-estimator to implicitly alleviate the influence of a sequence of potentially erroneous GPS and magnetometer measurements. Instead of minimizing the sum of squared residual, we, hence, propose the use of robust norm function $\rho(.)$ in our non-linear optimization problem. Examples of such robust $\rho(.)$ are l_1, Huber and Cauchy norm [42]. Note that we robustify our non-linear optimization problem using Cauchy norm (16) which leads to (17).

$$\rho(x) = \log(1 + x). \tag{16}$$

We propose the following robust non-linear least squares function that fuse IMU, GPS and magnetometer which arrive at different rates:

$$\begin{aligned}\min_{\hat{\boldsymbol{\chi}}_t} \frac{1}{2} \sum_{t=T-\mathrm{N}}^{T} \Bigg(& \left\| \mathbf{r}_{\mathrm{IMU}}(\mathbf{z}_{\mathrm{IMU}t\to t+1}, \hat{\boldsymbol{\chi}}_t) \right\|^2_{\boldsymbol{\Sigma_i}} \\ & + \rho\left(\left\| \mathbf{r}_{\mathrm{GPS}}(\mathbf{z}_{\mathrm{GPS}}, \hat{\boldsymbol{\chi}}_t) \right\|^2_{\boldsymbol{\Sigma_b}} \right) + \left\| \mathbf{r}_{\mathrm{B}}(\mathbf{z}_{\mathrm{B}}, \hat{\boldsymbol{\chi}}_t) \right\|^2_{\boldsymbol{\Sigma_c}} \\ & + \sum_{{}_b\tilde{\mathbf{m}}_k \in \Lambda} \rho\left(\left\| \mathbf{r}_{\mathrm{Mag}}(\mathbf{z}_{\mathrm{Mag}}, \hat{\boldsymbol{\chi}}_t) \right\|^2_{\boldsymbol{\Sigma_d}} \right) \Bigg), \end{aligned} \tag{17}$$

where N indexes all nodes in the window and Λ denotes the set of magnetometer measurement received.

To achieve real time processing time, the proposed method optimizes over a bounded N size sliding window of recent states. Note that each term of (17) is weighed by the sensor's noise covariances matrices $\boldsymbol{\Sigma}$. [2]

Also, note that the optimization problem (17) can be solved via generic least square solvers [26]–[28]. In Section

[2] In the case of IMU, readers can find the derivation of the pre-integrated covariance in [25].

V, we demonstrate that the above mentioned robustification successfully removes GPS outliers in real scenarios.

V. EXPERIMENTAL RESULTS

This section presents a number of experimental results to compare our proposed robust state estimation approach against a popular EKF implementation for Unmanned Aerial Vehicles (UAV), namely Autopilot [43], as the baseline. Owing to the fact that Autopilot has a large community of users including researchers, ordinary and commercial consumers, we regard this baseline as the current industrial state-of-the-art. The Autopilot EKF is designed with a threshold based outlier rejection. The strategy in the EKF is to use the ratio of the norm of the EKF innovation term to the observation variance to determine if the candidate observation is within a predefined confidence interval.

Besides that, we also regard [30]–[32] as the baseline methods. Since none of these works have considered scenarios involving measurement anomalies, we examine the sensitivity of their approaches (i.e., standard non-linear least squares) towards outliers. Also, as explained in Section I, their strategies in handling sensor asynchrony have fundamental weaknesses (vulnerable to wrong interpolation, a much larger set of variables to optimize), therefore, this aspect of their work is not tested in our experiments.

Since there is no openly available dataset that contains both an accurate (independently measured) ground truth information and all the sensory data that we require, i.e. IMU, magnetometer, and GPS, we provide two sets of experiments each aiming at illustrating different aspects of the comparison.

The first set of experiment is performed on the EuRoC Dataset [44]. The dataset is recorded indoor with a Micro Aerial Vehicle equipped with a low cost MEMS IMU. Corresponding 6D ground truth poses are provided by a Vicon system. Large IMU biases are observed in these datasets. The purpose of this experiment is to compare the performance of our proposed approach with the existing filtering method in a controlled environment where ground truth is available. The disadvantage of this dataset is that it does not contain real magnetometer (presumably, due to high magnetic disturbances indoor) and GPS measurements. To address this problem, we synthetically generate magnetometer and GPS measurements corresponding to the datasets, using the available data.

The second set of experiment is performed on real flight data using onboard sensory data log of actual autonomous flights performed outdoor. This dataset contains all of the required sensory data, including the magnetometer, but does not include an independently measured ground truth information (as it is outdoor). Despite the lack of ground truth to evaluate absolute accuracy, this dataset permits a qualitative comparison. Levenberg-Marquadt algorithm is applied to solve the nonlinear optimization problem (17). In all of our experiments, we use Ceres Solver [28].

A. Initialisation

For our proposed method, we assume no prior information is available about the states and we initialise every new state to the origin, i.e. $\mathbf{R}^w_{b_0} = \mathbf{I}$, ${}_w\mathbf{v}_0 = [0,0,0]^T$, ${}_w\mathbf{p}_0 = [0,0,0]^T$ and $\mathbf{b}^g_0 = [0,0,0]^T$. A more sophisticated initialisation could be employed, but, we try to consider the worst case scenario for our method. For the EKF, however, we initialise the pose and velocity to the ground truth, but we initialise the unknown bias to zero. Even though such setting gives an advantage to the EKF, this has been chosen intentionally to prevent EKF from divergence. Also, this highlights that our least squares approach is far more robust and does not necessarily require accurate initialization.

B. Size of window

We employ N = 40 in all of our experiments. It has been tuned carefully to achieve an optimum trade-off between the accuracy and the test time.

C. EuRoC Dataset Simulation

IMU measurements, ${}_b\tilde{\boldsymbol{\omega}}$ and ${}_b\tilde{\mathbf{a}}$, are sampled at 200Hz and perturbed by an additive noise of 0.0024rad/s and 0.0283m/s^2 respectively in each axis. Raw GPS/barometer and magnetometer measurements log are not available in this dataset. To generate barometer and GPS data, we corrupt the ground truth velocity and position measurements with Gaussian noise. We consider zero mean Gaussian noise with a standard deviation of 0.01m, and a sampling rate of 5Hz for barometer altitude. The noise signal with a standard deviation of 0.1m/s is selected for GPS velocity and 0.1m for position NE, and they are sampled at 5Hz. To simulate magnetometer measurements, we consider the normalized reference direction $\mathring{\mathbf{y}}(\mathrm{t}) = [1,0,0]^T$. We use (1) to generate ideal vector measurements, which are sampled at 100Hz. Zero mean Gaussian noise with a standard deviation of 0.01 is added to each axis of the resulting vector measurement. We evaluate the results on three sequences of the EuRoC dataset; V2_01_Easy, V2_02_Med, MH_03_Med. Two experiments are conducted, i.e., one without while another with outliers.

1) Scenario without outliers: Fig. 1 depicts the pose, velocity and bias estimates as well as their corresponding errors of our proposed algorithm compared with EKF in sequence MH_03_Med. The translation, velocity and bias estimation errors are simply the Euclidean norm of the error between the ground truth and the corresponding estimate. The attitude estimation error corresponds to the angle of rotation of the error $\hat{\mathbf{R}}(t)\mathbf{R}(t)^T$, where $\hat{\mathbf{R}}$ is the estimated orientation and

TABLE I: RMS Error of the proposed approach and the EKF [43] on three different EuRoC Sequences

Sequence	RMSE of	Attitude (deg)	Translation (m)	Velocity (m/s)	Bias (rad/s)
V2_01_Easy	EKF	1.0729	0.3438	0.1577	0.0435
	Proposed	**0.5770**	**0.0859**	**0.1249**	**0.0024**
V2_02_Med	EKF	0.9594	0.1753	0.1267	0.0476
	Proposed	**0.6976**	**0.0891**	**0.1155**	**0.0028**
MH_03_Med	EKF	1.3631	0.1639	0.1339	0.0406
	Proposed	**0.4579**	**0.0567**	**0.0707**	**0.0017**

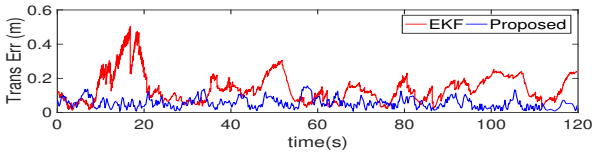

(a) Translation Error.

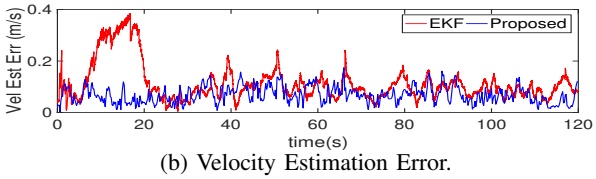

(b) Velocity Estimation Error.

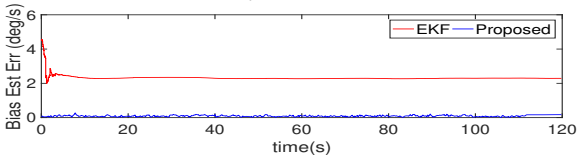

(c) Bias Estimation Error.

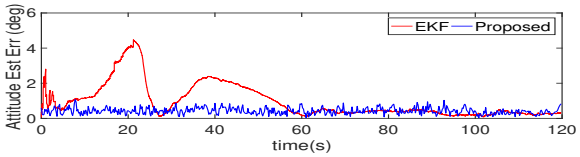

(d) Attitude Estimation Error.

Fig. 1: MH_03_Med - Comparison between our proposed approach and the EKF.

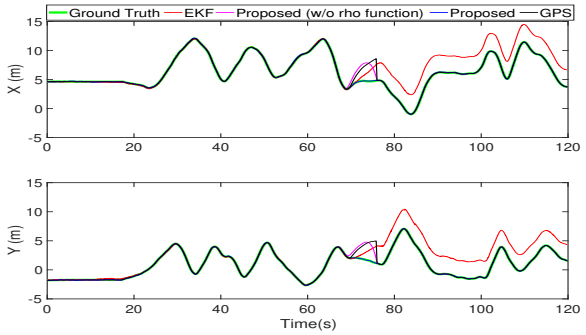

(a) **Top**: Position X Estimates. **Down**: Position Y Estimates.

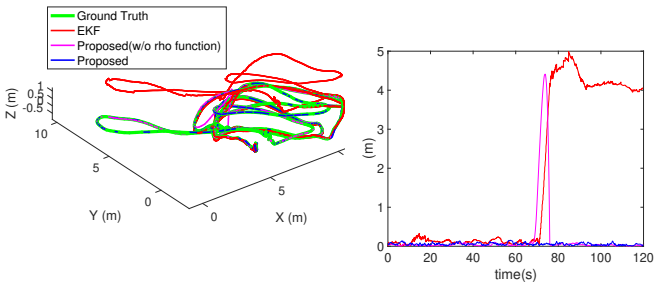

(b) **Left**: 3D view of the trajectory. **Right**: Translation Error.

Fig. 2: Seq MH_03_Med - Ground truth position XYZ vs their estimates via the EKF, the proposed method with ρ (rho) function disabled and the proposed method when measurement outliers occur from $t = 70$s to 76s.

$\mathbf{R}$ is its corresponding ground truth orientation. [3] The error plots show that our approach produces significantly lower errors than EKF. This is also confirmed by the rms error of the proposed approach versus EKF presented in Table I, which shows that the non-linear optimization function may offer better advantages in providing more accurate solution as computing the estimates at every iteration has the benefit of *gaining insight from a sequence of "raw" data quality* that is not possible in filtering approach.

2) Scenario with outliers: Fig. 2 compares the proposed approach (denoted by the blue line) with EKF when GPS position measurements are corrupted with outliers (denoted by the black line) from t = 70s to t = 76s. Throughout the flight of a total trajectory of 130.9m, it is observed that during the period when measurement outliers occur, our method tracks the true trajectory more accurately than EKF. In fact, the outlier identification method of EKF fails to isolate some of the outliers and the EKF incorrectly fuses them, as is evident by the fact that EKF position estimate (denoted by the red line) follows the black line as seen in Fig. 2a. This explains the slowly varying translation error of EKF. Also, this causes an adverse effect on EKF estimates even after t=76s when there is no more outlier. The EKF wrongly rejects healthy GPS measurements after (t=76s onwards) and relies mostly on dead reckoning, which leads to a significant deviation from the ground truth. In this experiment, we also assess the sensitivity of approach in [30]–[32] towards outliers by implementing (3) (denoted by the magenta line). Fig. 2 also presents a notable evidence that the resulting position estimates are distinctly biased to the measurement outliers without incorporating the robust norm function in the nonlinear least squares. Nevertheless, they still track the true pose closely once the GPS measurements become trustworthy again.

We also perform a Monte Carlo analysis with 50 simulation runs, each with randomised outlier insertion to the GPS position measurement. Fig. 3 presents a substantial evidence on the robustness of our approach as the r.m.s error averaged over 50 runs is lower compared to the EKF.

3) Timing: The experiment is implemented on a standard laptop (Macbook Pro, Intel i5, 2.3GHz) and is running on single core. As shown in Fig. 4, the average CPU time per window for the proposed approach over 50 Monte Carlo

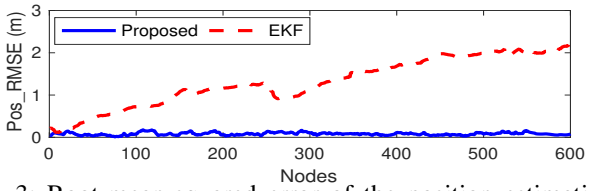

Fig. 3: Root-mean-squared error of the position estimation averaged over 50 Monte Carlo experiments with randomised outlier insertion.

[3] This angle is related to the Frobenius norm $\|I_3 - \hat{\mathbf{R}}\mathbf{R}^T\|_F^2 = tr((\mathrm{I} - \hat{\mathbf{R}}\mathbf{R}^T)^T(\mathrm{I} - \hat{\mathbf{R}}\mathbf{R}^T))$ and is given by $\tilde{\theta}(t) = \frac{180}{\pi} * \mathrm{acos}(1 - 0.25\|\mathrm{I} - \hat{\mathbf{R}}(t)\mathbf{R}(t)^T\|_F^2)$.

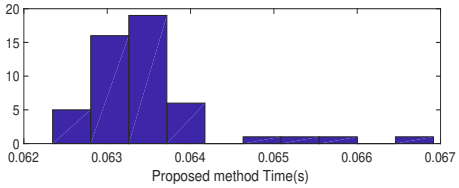

Fig. 4: Histogram plot of average CPU time per window for the proposed approach over 50 Monte Carlo runs.

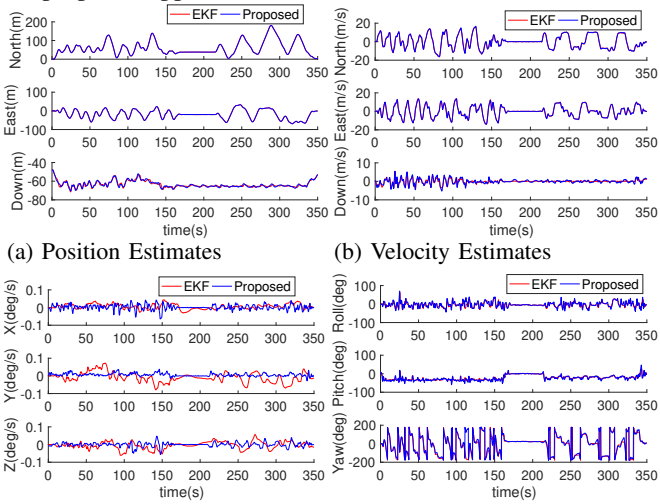

(a) Position Estimates (b) Velocity Estimates

(c) Bias Estimates (d) Attitude Estimates

Fig. 5: Real flight dataset-The estimation results via the proposed method and EKF.

runs is approximately 60ms, which matches the real-time constraints in our problem setup.

D. PX4 flight data

The second experiment is performed on the real flight data. The dataset is recorded with a F450-Pixhawk4 that is equipped with an IMU, a magnetometer, a GPS unit and a barometer.[4] The IMU is sampled at 250Hz while the magnetometer and GPS/barometer measurements are sampled at 50Hz and 5Hz, respectively. Again, we consider two scenarios for the real flight data as discussed in Sec. V-D.1 and V-D.2.

1) Scenario without outliers: As depicted in Fig. 5, the resulting state estimates of our proposed approach match very well with those of EKF. Note that there is no ground truth available in this dataset. As there is no outlier, we believe that the EKF estimates are reliable in Fig. 5.

2) Scenario with outliers: Fig. 6a illustrates the estimates of the proposed approach compared with EKF and (outlier-free) GPS measurements when GPS sensor fault occurs from t = 213s to 220s. Incorrect fusion of the measurement outliers (denoted by the black line) even for only a very short period of time has led to a very severe long term effect on EKF's performance. Contrarily, the resulting UAV's trajectory of our proposed approach still matches the trajectory path of (outlier-free) GPS measurements in the inset figure. Therefore, we highlight that our method demonstrate excellent robustness and performance in mitigating outliers compared with EKF. Fig. 6b compares the resulting position estimates under scenario with and without robust $\rho(.)$. We emphasise that incorporating robust norm in the nonlinear least squares for the state estimation is practically important to ensure long term autonomous navigation in a large scale environment.

[4]The dataset is available at: https://logs.px4.io/plot_app?log=114d429c-d4f6-43e6-b3b4-740bab900d2a.

VI. Conclusion

Aiming to offer a fresh insight to address the long standing pose estimation problem in INS/GPS fusion, we present a novel non-linear optimization framework to solve the equivalent problem. We extend the pre-integration technique to fuse different sensory inputs that arrive at different rates in a non-linear least squares optimisation framework. We also present a robust estimation framework to effectively mitigate the effects of practically important outlier measurements. Our experimental results demonstrate the superior accuracy and robustness of our approach over filtering methods. This further illustrate the huge potential of non-linear optimization approach in long term autonomous INS/GPS navigation.

References

[1] J. L. Crassidis, F. L. Markley, and Y. Cheng, "Survey of Nonlinear Attitude Estimation Methods," *Journal of guidance, control, and dynamics*, vol. 30, no. 1, pp. 12–28, 2007.

[2] A. Khosravian, "State Estimation for Systems on Lie groups with Nonideal Measurements," Ph.D. dissertation, The Australian National University (Australia), 2016.

[3] G. S. Chirikjian, *Stochastic Models, Information Theory, and Lie Groups, Volume 2: Analytic Methods and Modern Applications*. Springer Science & Business Media, 2011, vol. 2.

[4] S. Bonnabel, P. Martin, and P. Rouchon, "A non-linear symmetry-preserving observer for velocity-aided inertial navigation," in *American Control Conf.*, 2006, pp. 2910–2914.

[5] R. Mahony, T. Hamel, and J.-M. Pflimlin, "Nonlinear Complementary Filters on the Special Orthogonal Group," *IEEE Trans. on Automatic Control*, vol. 53, no. 5, pp. 1203–1218, 2008.

[6] T. H. Bryne, J. M. Hansen, R. H. Rogne, N. Sokolova, T. I. Fossen, and T. A. Johansen, "Nonlinear Observers for Integrated INS/GNSS Navigation: Implementation Aspects," *IEEE Control Systems*, vol. 37, no. 3, pp. 59–86, 2017.

[7] G. Agamennoni, J. I. Nieto, and E. M. Nebot, "An outlier-robust Kalman filter," in *IEEE Intl. Conf. on Robotics and Automation (ICRA)*, 2011.

[8] A. Ali, S. Siddharth, Z. Syed, and N. El-Sheimy, "Swarm Optimization-Based Magnetometer Calibration for Personal Handheld Devices," *Sensors*, vol. 12, no. 9, pp. 12 455–12 472, 2012.

[9] H. F. Grip, T. I. Fossen, T. A. Johansen, and A. Saberi, "Globally exponentially stable attitude and gyro bias estimation with application to GNSS/INS Integration," *Automatica*, vol. 51, pp. 158–166, 2015.

[10] A. Roberts and A. Tayebi, "On the attitude estimation of accelerating rigid-bodies using GPS and IMU measurements," in *IEEE Conf. on Decision and Control and European Control Conf. (CDC-ECC)*, 2011, pp. 8088–8093.

[11] A. Barrau and S. Bonnabel, "The Invariant Extended Kalman Filter as a stable observer," *IEEE Trans. on Automatic Control*, vol. 62, no. 4, pp. 1797–1812, 2017.

[12] J. F. Vasconcelos, C. Silvestre, and P. Oliveira, "A Nonlinear GPS/IMU based observer for rigid body attitude and position estimation," in *IEEE Conf. on Decision and Control (CDC)*, 2008, pp. 1255–1260.

[13] M. Izadi, A. K. Sanyal, E. Barany, and S. P. Viswanathan, "Rigid Body Motion Estimation based on the Lagrange-d'Alembert principle," in *IEEE Conf. on Decision and Control (CDC)*, 2015, pp. 3699–3704.

[14] H. Rehbinder and B. K. Ghosh, "Pose estimation using line-based dynamic vision and inertial sensors," *IEEE Trans. on Automatic control*, vol. 48, no. 2, pp. 186–199, 2003.

[15] D. Senejohnny and M. Namvar, "A predictor-based attitude and position estimation for rigid bodies moving in planar space by using delayed landmark measurements," *Robotica*, vol. 35, no. 6, pp. 1415–1430, 2017.

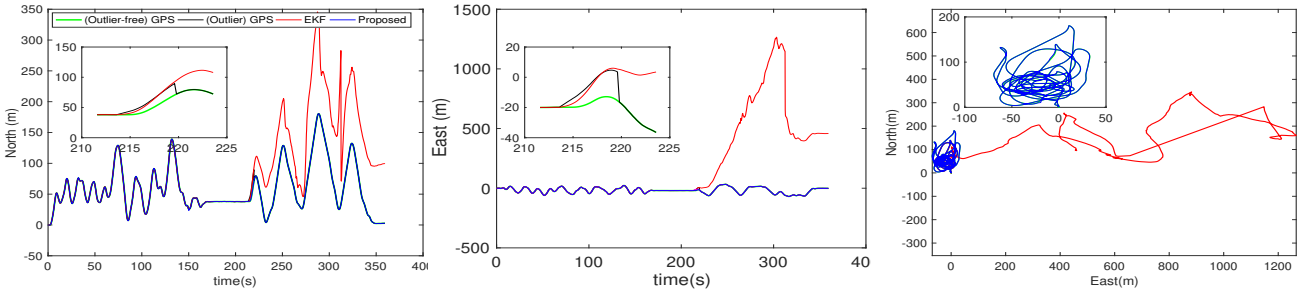

(a) **Left**, **Center**: Position estimates; **Right**: Estimated trajectory; of the EKF, our proposed method with ρ (rho) function versus (outlier-free) GPS measurements.

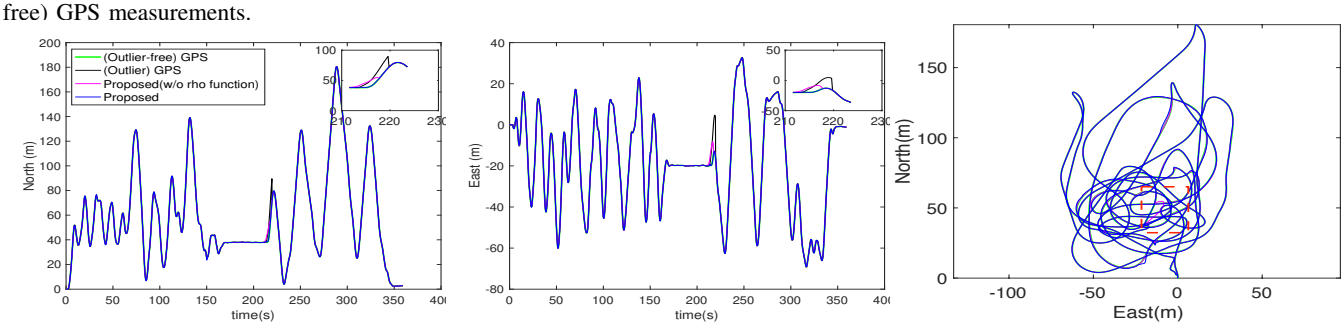

(b) **Left**, **Center**: Position estimates; **Right**: Estimated trajectory; of our proposed method with and without ρ (rho) function versus (outlier-free) GPS measurements. The inset figure (**Left,Center**) shows that with the $\rho(.)$-disabled approach, the resulting position estimates are biased to the GPS outliers. Also, take note the incorrect trajectory (denoted by the square bracket) on the **Right**.

Fig. 6: Estimated Position and the corresponding trajectory when measurement outliers occur from t = 213(s) to t = 220(s).

[16] R. Mahony, T. Hamel, and J.-M. Pflimlin, "Complementary filter design on the special orthogonal group SO(3)," in *Proc. of the IEEE Transactions on Decision and Control, CDC*, 2005.

[17] L. A. McGee and S. F. Schmidt, "Discovery of the Kalman filter as a practical tool for aerospace and industry," NASA Ames Research Center, Tech. Rep. 86847, 1985.

[18] M. A. Gandhi, "Robust Kalman filters using generalized maximum likelihood-type estimators," Ph.D. dissertation, Virginia Tech, 2009.

[19] S. Thrun, W. Burgard, and D. Fox, *Probabilistic robotics*. MIT press, 2005.

[20] J.-A. Ting, E. Theodorou, and S. Schaal, "A Kalman filter for robust outlier detection," in *IEEE/RSJ Intl. Conf. on Intelligent Robots and Systems (IROS)*, 2007.

[21] B. Kovačević, Ž. Đurović, and S. Glavaški, "On robust Kalman filtering," *Intl. Journal of Control*, vol. 56, no. 3, pp. 547–562, 1992.

[22] H. Strasdat, J. Montiel, and A. J. Davison, "Real-time monocular SLAM: Why filter?" in *IEEE Intl. Conf. on Robotics and Automation (ICRA)*, 2010.

[23] S. Leutenegger, S. Lynen, M. Bosse, R. Siegwart, and P. Furgale, "Keyframe-based visual-inertial odometry using nonlinear optimization," *The Intl. Journal of Robotics Research*, vol. 34, no. 3, pp. 314–334, 2015.

[24] G. P. Huang, A. I. Mourikis, and S. I. Roumeliotis, "An observability-constrained sliding window filter for SLAM," in *IEEE/RSJ Intl. Conf. on Intelligent Robots and Systems (IROS)*, 2011.

[25] C. Forster, L. Carlone, F. Dellaert, and D. Scaramuzza, "IMU Preintegration on Manifold for Efficient Visual-Inertial Maximum-a-Posteriori Estimation," in *Robotics: Science and Systems*, 2015.

[26] R. Kümmerle, G. Grisetti, H. Strasdat, K. Konolige, and W. Burgard, "g2o: A General Framework for Graph Optimization," in *IEEE Intl. Conf. on Robotics and Automation (ICRA)*, 2011.

[27] F. Dellaert, "Factor graphs and GTSAM: A Hands-on introduction," Georgia Institute of Technology, Tech. Rep., 2012.

[28] S. Agarwal, K. Mierle, *et al.* (2012) Ceres Solver. [Online]. Available: http://ceres-solver.org

[29] J. Vandersteen, M. Diehl, C. Aerts, and J. Swevers, "Spacecraft Attitude Estimation and Sensor Calibration Using Moving Horizon Estimation," *Journal of Guidance, Control, and Dynamics*, vol. 36, no. 3, pp. 734–742, 2013.

[30] T. Polóni, B. Rohal-Ilkiv, and T. A. Johansen, "Moving Horizon Estimation for Integrated Navigation Filtering," *IFAC-PapersOnLine*, vol. 48, no. 23, pp. 519–526, 2015.

[31] F. Girrbach, J. D. Hol, G. Bellusci, and M. Diehl, "Optimization-based Sensor Fusion of GNSS and IMU Using a Moving Horizon Approach," *Sensors*, vol. 17, no. 5, p. 1159, 2017.

[32] F. Girrbach, J. D. Hol, G. Bellusci, and M. Diehl, "Towards robust sensor fusion for state estimation in airborne applications using GNSS and IMU," *IFAC-PapersOnLine*, vol. 50, no. 1, pp. 13 264–13 269, 2017.

[33] P. Martin and E. Salaün, "An invariant observer for earth-velocity-aided attitude heading reference systems," *IFAC Proceedings Volumes*, vol. 41, no. 2, pp. 9857–9864, 2008.

[34] P. Martin and E. Salaün, "Design and implementation of a low-cost observer-based attitude and heading reference system," *Control Engineering Practice*, vol. 18, no. 7, pp. 712–722, 2010.

[35] P. E. Crouch and R. Grossman, "Numerical integration of ordinary differential equations on manifolds," *Journal of Nonlinear Science*, vol. 3, no. 1, pp. 1–33, 1993.

[36] H. Munthe-Kaas, "High order runge-kutta methods on manifolds," *Applied Numerical Mathematics*, vol. 29, no. 1, pp. 115–127, 1999.

[37] J. Park and W.-K. Chung, "Geometric integration on euclidean group with application to articulated multibody systems," *IEEE Trans. Robotics*, vol. 21, no. 5, pp. 850–863, 2005.

[38] M. S. Andrle and J. L. Crassidis, "Geometric integration of quaternions," *Journal of Guidance, Control, and Dynamics*, vol. 36, no. 6, pp. 1762–1767, 2013.

[39] C. Forster, L. Carlone, F. Dellaert, and D. Scaramuzza, "On-manifold preintegration for real-time visual–inertial odometry," *IEEE Trans. Robotics*, vol. 33, no. 1, pp. 1–21, 2017.

[40] A. Khosravian, J. Trumpf, R. Mahony, and C. Lageman, "Observers for invariant systems on Lie groups with biased input measurements and homogeneous outputs," *Automatica*, vol. 55, pp. 19–26, 2015.

[41] C. Le Gentil, T. Vidal-Calleja, and H. Shoudong, "3D Lidar-IMU calibration based on upsampled preintegrated measurements for motion distortion correction," in *IEEE Intl. Conf. on Robotics and Automation (ICRA)*, 2018.

[42] K. Aftab and R. Hartley, "Convergence of Iteratively Re-weighted Least Squares to Robust M-Estimators," in *IEEE Conf. on Applications of Computer Vision (WACV)*, 2015, pp. 480–487.

[43] (2018) PX4 Autopilot. [Online]. Available: https://dev.px4.io

[44] M. Burri, J. Nikolic, P. Gohl, T. Schneider, J. Rehder, S. Omari, M. W. Achtelik, and R. Siegwart, "The EuRoc micro aerial vehicle datasets," *The Intl. Journal of Robotics Research*, vol. 35, no. 10, pp. 1157–1163, 2016.